AIP | Applied Physics Letters

Non-contact optoacoustic imaging with focused air-coupled transducers

X. Luís Deán-Ben, Genny A. Pang, Francisco Montero de Espinosa, and Daniel Razansky

Citation: Applied Physics Letters **107**, 051105 (2015); doi: 10.1063/1.4928123
View online: http://dx.doi.org/10.1063/1.4928123
View Table of Contents: http://scitation.aip.org/content/aip/journal/apl/107/5?ver=pdfcov
Published by the AIP Publishing

Non-contact optoacoustic imaging with focused air-coupled transducers

X. Luís Deán-Ben,[1] Genny A. Pang,[1,2] Francisco Montero de Espinosa,[3] and Daniel Razansky[1,2,a)]
[1]*Institute for Biological and Medical Imaging (IBMI), Helmholtz Zentrum München, Neuherberg, Germany*
[2]*School of Medicine, Technische Universität München (TUM), Munich, Germany*
[3]*CSIC, Institute of Physics and Communication Technologies, Madrid, Spain*

(Received 13 May 2015; accepted 21 July 2015; published online 5 August 2015)

Non-contact optoacoustic imaging employing raster-scanning of a spherically focused air-coupled ultrasound transducer is showcased herein. Optoacoustic excitation with laser fluence within the maximal permissible human exposure limits in the visible and near-infrared spectra is applied to objects with characteristic dimensions smaller than 1 mm and absorption properties representative of the whole blood at near-infrared wavelengths, and these signals are shown to be detectable without contact to the sample using an air-coupled transducer with reasonable signal averaging. Optoacoustic images of vessel-mimicking tubes embedded in an agar phantom captured with this non-contact sensing technique are also showcased. These initial results indicate that an air-coupled ultrasound detection approach can be suitable for non-contact biomedical imaging with optoacoustics.
 [http://dx.doi.org/10.1063/1.4928123]

Biomedical optoacoustic imaging has developed as a capable biomedical imaging technique owing to the powerful combination of rich optical absorption contrast and high spatial resolution attained on the millimeter to centimeter penetration depth scales into scattering biological tissues.[1,2] A handful of new applications in pre-clinical research have been recently enabled by optoacoustics[3–5] and several dedicated systems have been further developed to facilitate efficient clinical translation of this modality.[6–9] Much like in ultrasonography, optoacoustic imaging techniques rely on ultrasound transmission from the optical absorbers located within the imaged tissues to the detection locations surrounding the imaged area. Direct physical contact of the acoustic detectors with the tissue or an impedance matching medium (typically water) is commonly achieved in order to enable efficient detection of optoacoustic responses with piezoelectric transducers.[10–12] However, in applications like open surgeries, imaging of burns, or other lesions, this contact nature of optoacoustics may present significant limitations as compared to other non-contact imaging modalities such as optical imaging, X-Ray computed tomography, or magnetic resonance imaging.

Detection of optoacoustically induced ultrasound waves from remote locations was previously shown possible with optical methods, including optical interferometry[13–16] and beam deflection approaches.[17] These techniques are generally based on the measurement of surface displacement, so that detection of further ultrasound propagation outside the imaged body is not required. However, surface irregularities hamper applicability of a fully non-contact interferometric detection when applied to real biological tissues; thus, optical interferometry is usually done with resonant films in direct contact with the surface of the imaged object[18] or with immersed fiber-based detectors.[19]

Air-coupled transducers are an alternative method capable of non-contact ultrasound detection and have been previously applied for non-destructive testing and material characterization. In the case of low ultrasonic frequencies, micro-membrane capacitance transducers are the best choice for air-coupled detection,[20,21] whereas at frequencies above 1 MHz piezoelectric transducers adapted to air by using microporous coupling layers are more convenient, mainly because focused apertures and array configurations can be readily realized for improved sensitivity.[22] The main limitation associated with coupling of ultrasound through air is the large acoustic impedance mismatch of air with biological tissues that have acoustic properties similar to water. Moreover, the high attenuation of ultrasonic waves in air of 1.6 dB/cm for 1 MHz frequency components[23] also contributes to difficulties detecting optoacoustic signals without direct contact. In spite of these challenges, feasibility of detecting optoacoustic signals in a single dimension through air has been demonstrated when a large laser excitation fluence is used to excite a highly absorbing medium.[24] Optoacoustic imaging using non-contact sensors and laser excitation within the maximum permissible human exposure limits (20 mJ/cm^2 energy per pulse and 200 mW/cm^2 average power for both visible and near-infrared wavelengths), however, has never been presented till date. In this letter, we showcase the feasibility of optoacoustic imaging of blood-equivalent optical absorbers using spherically focused air-coupled transducers while employing light fluence levels below the safety standards for human exposure to pulsed laser radiation.

The lay-out of the experimental system is depicted in Fig. 1(a). Phantoms consisting of 1 cm thick clear agar blocks containing ink-filled cylindrical channels were used. The agar matrix consists of 1.3% agar powder (by weight) in distilled water. The phantoms are transparent and have a speed of sound of approximately 1500 m/s. Different dilutions of ink (Higgins, Chartpak, Inc.) were imaged in channels of varying diameters between 0.5 and 2 mm. The ink channels were positioned at a very shallow depth (approximately 1 mm) from the side of the agar surface facing the acoustic transducer. A self-developed spherically focused

a)Electronic mail: dr@tum.de

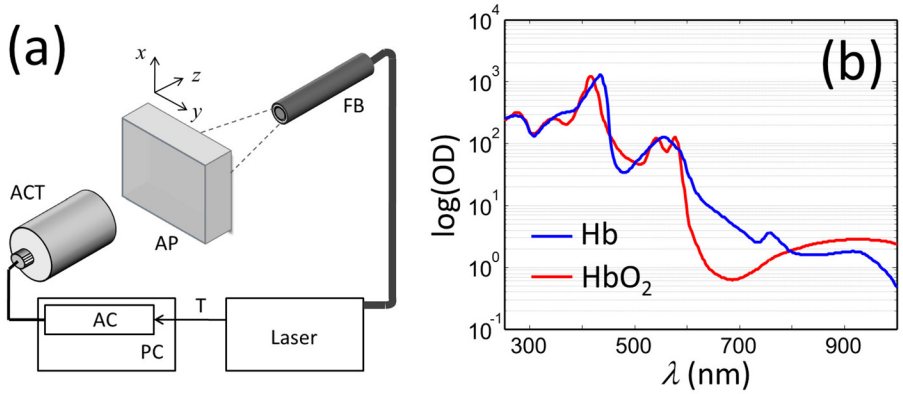

FIG. 1. (a) Layout of the experimental setup, ACT (air-coupled transducer), AP (agar phantom), FB (fiber bundle), PC (personal computer), AC (acquisition card), T (trigger). (b) Optical density of oxygenated (HbO_2) and deoxygenated (Hb) hemoglobin for a typical concentration of 150 g/l in blood as a function of the optical wavelength.

piezoelectric air-coupled transducer with a central frequency of 800 kHz and a −6 dB bandwidth of 400 kHz (20 mm diameter of the active area, 25 mm focal distance) was positioned at a distance of approximately 25 mm from the surface of the phantom. The transducer is based on a 1–3 piezocomposite adapted to air with two one quarter wavelength matching layers. The first layer consists of the same material as the piezocomposite (Araldite D), whereas the second layer is a microporous cellulose membrane (Millipore). No backing is used. The use of a piezocomposite instead of a piezoceramic disc is required to increase the efficiency and frequency bandwidth as well as to shape the transducer to the desired focusing geometry. The optical illumination was achieved with an optical parametric oscillator (OPO)-based laser (Innolas Laser GmbH, Krailling, Germany) directed on the opposite side of the agar as the acoustic sensor. A light beam at 750 nm wavelength was guided through a custom-made fiber bundle (CeramOptec GmbH, Bonn, Germany) delivering approximately 12 mJ to the imaged sample. The output of the bundle was positioned in close proximity to the surface of the phantom, so that the diameter of the light beam at the ink channel was approximately 9 mm^2, corresponding to excitation light fluence of 20 mJ/cm^2. The phantoms were attached to a platform allowing for raster-scanning along x- and y-directions. The optoacoustic signals were digitized with an embedded acquisition card at 10 Megasamples per second and 12 bits vertical resolution (AlazarTech, ATS9351). The acquired signals were band-pass filtered between 600 and 1000 kHz to remove high frequency noise and low frequency offsets.

In an initial experiment, straight ink channels with diameters of 0.5 mm, 1 mm, and 2 mm aligned with the y-axis were imaged. The absorbance values A (or optical density OD) of the different ink dilutions tested in the channels were 2.5, 10, and 25, whereas the corresponding optical absorption coefficient μ_a can be calculated via $\mu_a = 2.3A/l$, where l is the length of the sample. For reference, the OD of oxygenated and deoxygenated hemoglobin for realistic concentration of 150 g/l in blood is displayed in Fig. 1(b). At the isosbestic wavelength of approximately 800 nm, the OD of hemoglobin is approximately 1.9, and the OD values for blood in the entire so-called near-infrared window of light (700–900 nm) are between 0.7 and 3. In this spectral range, optical absorption by water is minimized thus leading to an optimized penetration depth of light within biological tissues. Fig. 2 displays the time-resolved acoustic signals corresponding to the maximum detected amplitude, which occurs when the agar block is positioned such that the ink channel lies at the focal area of the transducer. Signals corresponding to the three different optical densities for the 1 mm diameter ink insertions are shown along with the effect of averaging of the signal. After 1000 averages, the signal originating from the ink channel is clearly visible at a time near 70 μs even for the lowest OD imaged; for the ink channels with higher OD, the signal can be clearly distinguished in as few as 10 averages. The measured time delay of 70 μs between the laser excitation and when the optoacoustic signal reaches the detector is in good agreement with the expected time-of-flight of the acoustic wave traveling through air from the agar block to the detector (approximately 25 mm, the focal distance of the transducer). The signal-to-noise ratio (SNR) for these signals as a function of the number of averages N is shown in Figs. 3(a)–3(c) for the different channel diameters and ink dilutions. Larger channels can be expected to generate higher signals because they contain a larger volume of absorbing ink, and this is confirmed in the results.

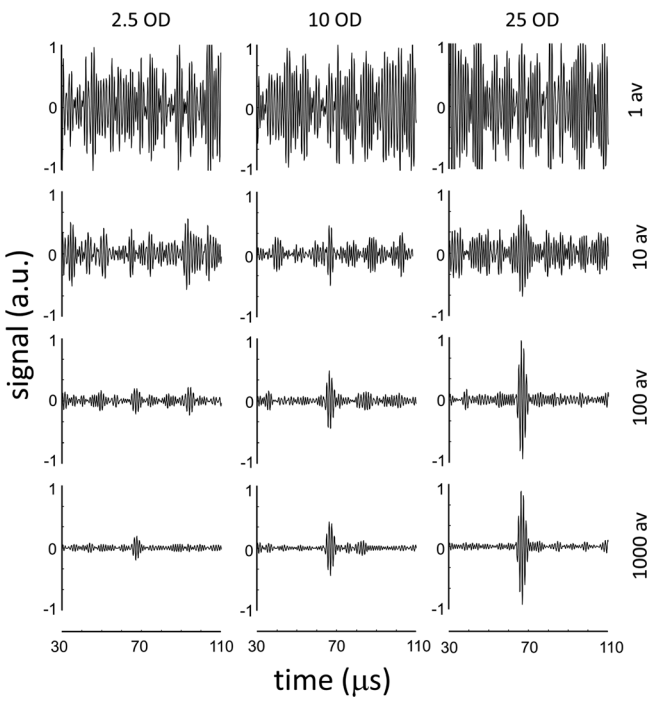

FIG. 2. Optoacoustic signals collected with the air-coupled transducer corresponding to a cylindrical ink channel with a diameter of 1 mm. Results for different optical densities of the ink channel are shown, as well as the effect of the number of averages on the signal.

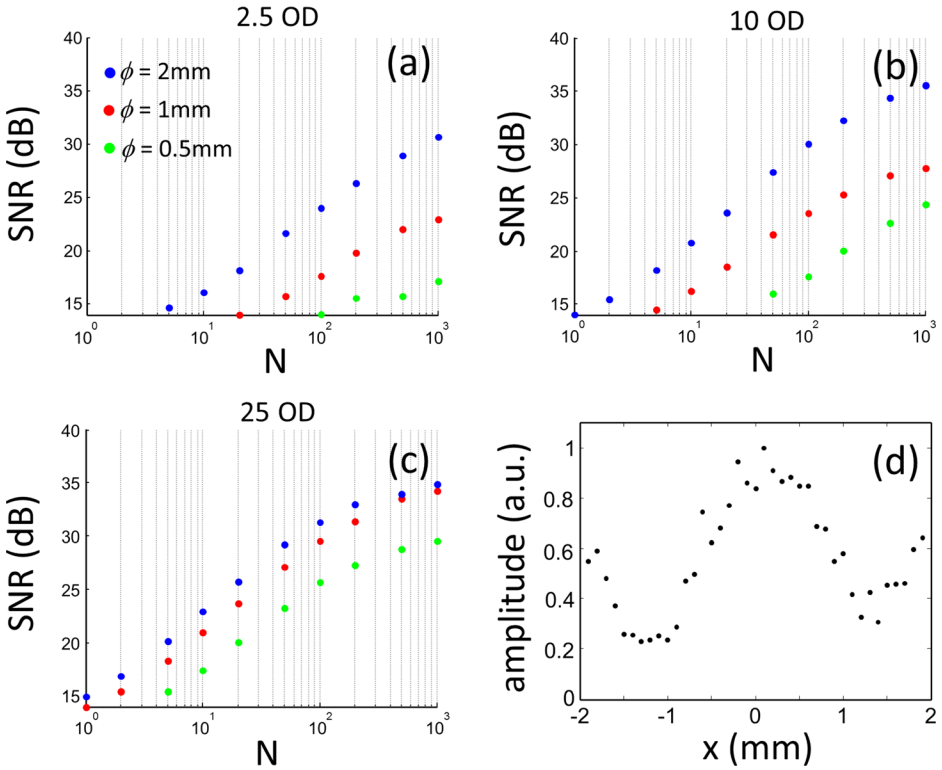

FIG. 3. (a)–(c) Signal-to-noise ratio of the optoacoustic signals for cylindrical ink insertions with diameters of 0.5 mm (green), 1 mm (red), and 2 mm (blue) as a function of the number of averages for three different values of the optical density. (d) Amplitude of the optoacoustic signal collected with the air-coupled transducer as a function of the lateral displacement for the ink insertion with 10 OD and a diameter of 0.5 mm.

The SNR can also be increased with more averages or higher optical density. The SNR was calculated as the ratio between the peak-to-peak amplitude for a time window of 9 μs centered around the instant corresponding to the maximum detected signal amplitude and the standard deviation of the background for a time window of 40 μs after arrival of the signal. Only SNR values above 14 dB are plotted, for which we considered that the signal can be distinguishable from the noise. To examine the spatial resolution capability of the imaging technique, the spherically focused detector was linearly translated along direction perpendicular to the straight ink channels, along the x-axis. The amplitude of the signals for the ink channel with 0.5 mm diameter and an OD of 10 as a function of the lateral scanning distance (x direction) is shown in Fig. 3(d). The full width at half maximum (FWHM) indicates the potential resolution that can be achieved. For instance, the FWHM of the 0.5 mm channel shown in Fig. 3(d) is 1.75 mm, indicating that the spatial resolution is higher than this value. Due to the use of the focused acoustic transducer, the measured FWHM will be also affected by the depth at which the absorber is located; the optimal resolution is expected at the focal plane of the transducer.

In order to demonstrate the basic imaging capability of the non-contact optoacoustic detection system, a phantom containing complex absorbing structures was raster scanned along both the x- and y-directions. The phantom contained straight and curved ink channels all with diameters 0.5 and 1 mm and OD of 10 arranged onto the z-axis plane of the transducer's focal point (approximately 1 mm from the phantom surface), as shown in Fig. 4(a). The scanning was performed with a step of 0.3 mm covering a total area of 12.3 $\times$ 7.5 mm^2. A two dimensional image was formed by considering the maximum peak-to-peak amplitude of the signals in the time window of 12 μs centered around the time point corresponding to the geometrical focus of the transducer. The resulting images formed using different numbers of averages are shown in Figs. 4(b)–4(e). Generally, good correspondence with the actual phantom geometry can be observed with improving image quality as the number of averages is increased. The spatial resolution of the resolved structures is influenced by the available detection bandwidth and aperture of the air-coupled transducer.

The showcased results demonstrate the feasibility of generating non-contact optoacoustic images by raster

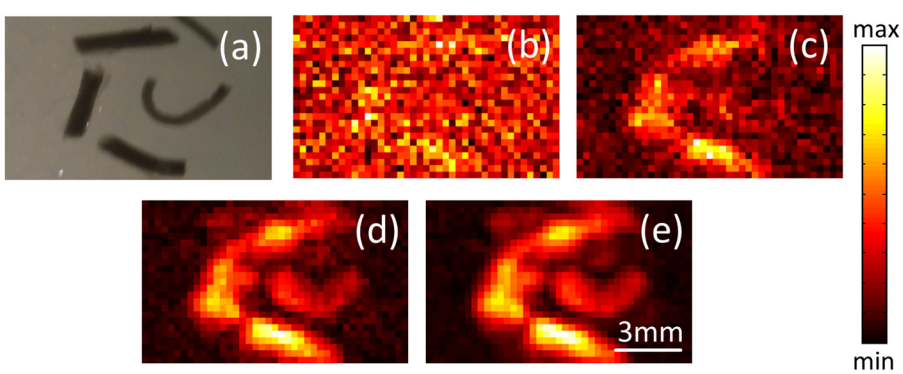

FIG. 4. Optoacoustic images obtained by raster scanning of the spherically focused air-coupled transducer. (a) Photograph of the imaged ink channels. (b)–(e) Optoacoustic images of the phantom after the recorded signals have been averaged 1, 10, 100, and 1000 times, respectively.

scanning of a spherically focused air-coupled transducer over absorbing structures with absorption properties similar to whole blood in the visible and near-infrared spectra, using only laser excitation energy within the recognized safety limits for human exposure. When applied to real tissue, the excitation light intensity will attenuate as it penetrates into scattering and absorbing medium, which will impact the effective number of signal averages needed for imaging at a given penetration depth. However, when imaging in the visible range of the optical spectrum, the OD of blood increases substantially, reaching values above 1000 at 420 nm, while the safety exposure limit remains at a constant value of 20 mJ/cm^2 across the entire visible spectrum.[25] Thereby, it can be expected that optoacoustic imaging with this air-coupled transducer approach in the visible wavelength range could be potentially performed with much fewer averages or none at all, in cases where only limited penetration depth is desired. Another potential concern that should be addressed is the axial resolution, which is inversely proportional to the detection bandwidth of the transducer.[26] Typically, immersion-based focused ultrasound transducers can be efficiently designed to achieve sensitive and broadband detection at relatively high frequencies, yielding good axial resolution performance. The air-coupled transducers employed in this work are characterized by a very narrow detection bandwidth, which significantly compromises the axial resolution performance.

Several important next steps that are required before this non-contact optoacoustic imaging method can be employed in pre-clinical and clinical uses include optimization of the geometry of the detector and frequency response, validating the feasibility to image real biological targets, and acceleration of the image acquisition time with multi-element arrays.[11,27] Optoacoustic tomographic approaches may also be possible with air-coupled transducers. In this context, arrays of air-coupled transducers have been so far developed for non-destructive testing applications,[28,29] yet their performance for optoacoustic imaging needs to be verified. For imaging real biological tissues and blood vessels, one would need to achieve a good balance between the SNR and imaging depth. In addition, multi-spectral imaging may be employed to improve detection sensitivity and to determine blood oxygen saturation. The latter aspect is important in clinical practice[30] and the non-contact nature of the suggested approach may facilitate emergence of clinical applications of optoacoustics.

In conclusion, non-contact optoacoustic imaging with air-coupled transducers in tissue-mimicking phantoms was demonstrated herein. These results suggest that optoacoustic systems can be designed with this detection technology, and the important advantages derived from the non-contact nature of this approach are expected to expand applicability of optoacoustic imaging in biological research and clinical practice.

G.A.P acknowledges the support from the Technical University of Munich University Foundation Fellowship. F.M.E. acknowledges the support from CICYT DPI2013-46915-C2-1-R Grant. D.R. acknowledges the support from the European Union under Grant Agreement No. ERC-2010-StG-260991.

[1]D. Razansky, "Multispectral optoacoustic tomography: Volumetric color hearing in real time," IEEE J. Sel. Top. Quantum Electron. **18**(3), 1234–1243 (2012).
[2]L. V. Wang and S. Hu, "Photoacoustic tomography: *in vivo* imaging from organelles to organs," Science **335**(6075), 1458–1462 (2012).
[3]S. Gottschalk, T. F. Fehm, X. L. Deán-Ben, and D. Razansky, "Noninvasive real-time visualization of multiple cerebral hemodynamic parameters in whole mouse brains using five-dimensional optoacoustic tomography," J. Cereb. Blood Flow Metab. **35**(4), 531–535 (2015).
[4]J. Yao, L. Wang, J.-Mo. Yang, K. I. Maslov, T. T. W. Wong, L. Li, C.-H. Huang, J. Zou, and L. V. Wang, "High-speed label-free functional photoacoustic microscopy of mouse brain in action," Nat. Methods **12**(5), 407–410 (2015).
[5]M. Omar, M. Schwarz, D. Soliman, P. Symvoulidis, and V. Ntziachristos, "Pushing the optical imaging limits of cancer with multi-frequency-band raster-scan optoacoustic mesoscopy (RSOM)," Neoplasia **17**(2), 208–214 (2015).
[6]J.-Mo. Yang, C. Favazza, R. Chen, J. Yao, X. Cai, K. Maslov, Q. Zhou, K. K. Shung, and L. V. Wang, "Simultaneous functional photoacoustic and ultrasonic endoscopy of internal organs *in vivo*," Nat. Med. **18**(8), 1297–1302 (2012).
[7]M. Heijblom, D. Piras, W. Xia, J. C. G. Van Hespen, J. M. Klaase, F. M. van den Engh, T. G. Van Leeuwen, W. Steenbergen, and S. Manohar, "Visualizing breast cancer using the Twente photoacoustic mammoscope: What do we learn from twelve new patient measurements?," Opt. Express **20**(11), 11582–11597 (2012).
[8]A. Dima and V. Ntziachristos, "Non-invasive carotid imaging using optoacoustic tomography," Opt. Express **20**(22), 25044–25057 (2012).
[9]X. L. Deán-Ben, E. Bay, and D. Razansky, "Functional optoacoustic imaging of moving objects using microsecond-delay acquisition of multispectral three-dimensional tomographic data," Sci. Rep. **4**, 5878 (2014).
[10]H.-P. Brecht, R. Su, M. Fronheiser, S. A. Ermilov, A. Conjusteau, and A. A. Oraevsky, "Whole-body three-dimensional optoacoustic tomography system for small animals," J. Biomed. Opt. **14**(6), 064007 (2009).
[11]T. F. Fehm, X. L. Deán-Ben, and D. Razansky, "Four dimensional hybrid ultrasound and optoacoustic imaging via passive element optical excitation in a hand-held probe," Appl. Phys. Lett. **105**(17), 173505 (2014).
[12]M. P. Fronheiser, S. A. Ermilov, H.-P. Brecht, A. Conjusteau, R. Su, K. Mehta, and A. A. Oraevsky, "Real-time optoacoustic monitoring and three-dimensional mapping of a human arm vasculature," J. Biomed. Opt. **15**(2), 021305 (2010).
[13]G. Rousseau, A. Blouin, and J.-P. Monchalin, "Non-contact photoacoustic tomography and ultrasonography for tissue imaging," Biomed. Opt. Express **3**(1), 16–25 (2012).
[14]Yi. Wang, C. Li, and R. K. Wang, "Noncontact photoacoustic imaging achieved by using a low-coherence interferometer as the acoustic detector," Opt. Lett. **36**(20), 3975–3977 (2011).
[15]S. J. Park, J. Eom, Y. Ho. Kim, C. Su. Lee, and B. Ha. Lee, "Noncontact photoacoustic imaging based on all-fiber heterodyne interferometer," Opt. Lett. **39**(16), 4903–4906 (2014).
[16]A. Hochreiner, J. Bauer-Marschallinger, P. Burgholzer, B. Jakoby, and T. Berer, "Non-contact photoacoustic imaging using a fiber based interferometer with optical amplification," Biomed. Opt. Express **4**(11), 2322–2331 (2013).
[17]E. Khachatryan, S. Maswadi, D. A. Tsyboulski, E. Barnes, A. A. Oraevsky, K. L. Nash, and R. D. Glickman, "Optoacoustic microscopy using laser beam deflection technique," Proc. SPIE **8943**, 89432T (2014).
[18]A. P. Jathoul, J. Laufer, O. Ogunlade, B. Treeby, B. Cox, E. Zhang, P. Johnson, A. R. Pizzey, B. Philip, T. Marafioti, *et al.*, "Deep *in vivo* photoacoustic imaging of mammalian tissues using a tyrosinase-based genetic reporter," Nat. Photonics **9**(4), 239–246 (2015).
[19]A. Rosenthal, D. Razansky, and V. Ntziachristos, "High-sensitivity compact ultrasonic detector based on a pi-phase-shifted fiber Bragg grating," Opt. Lett. **36**(10), 1833–1835 (2011).
[20]T.-H. Gan, D. A. Hutchins, D. R. Billson, and D. W. Schindel, "High-resolution, air-coupled ultrasonic imaging of thin materials," IEEE Trans. Ultrason. Ferroelectr. Freq. Control **50**(11), 1516–1524 (2003).
[21]A. O. Manzanares and F. Montero de Espinosa, "Air-coupled mumps capacitive micromachined ultrasonic transducers with resonant cavities," Ultrasonics **52**(4), 482–489 (2012).
[22]F. Montero de Espinosa, T. E. Gómez, A. Albareda, R. Perez, and J. A. Casals, "High sensitive piezoelectric transducers for NDE air borne applications," IEEE Int. Ultrason. Symp. **2**, 1073–1076 (2000).

[23]A. S. Birks, R. E. Green, and P. MacIntire, *ASNT Nondestructive Testing Handbook: Ultrasonic Testing*, Nondestructive Testing Handbook Vol. 7 (American Society for Nondestructive Testing, American Society for Metals, 1991).
[24]R. G. M. Kolkman, E. Blomme, T. Cool, M. Bilcke, T. G. van Leeuwen, W. Steenbergen, K. A. Grimbergen, and G. J. den Heeten, "Feasibility of noncontact piezoelectric detection of photoacoustic signals in tissue-mimicking phantoms," J. Biomed. Opt. **15**(5), 055011 (2010).
[25]ANSI Standard Z136. 1., *American National Standard for the Safe Use of Lasers* (American National Standards Institute, Inc., New York, 1993).
[26]L. V. Wang, "Tutorial on photoacoustic microscopy and computed tomography," IEEE J. Sel. Top. Quantum Electron. **14**(1), 171–179 (2008).
[27]A. Buehler, X. L. Deán-Ben, J. Claussen, V. Ntziachristos, and D. Razansky, "Three-dimensional optoacoustic tomography at video rate," Opt. Express **20**(20), 22712–22719 (2012).
[28]M. Akhnak, O. Martinez, L. G. Ullate, and F. Montero de Espinosa, "64 elements two-dimensional piezoelectric array for 3d imaging," Ultrasonics **40**(1), 139–143 (2002).
[29]M. J. Garcia-Hernandez, J. A. Chavez, Y. Yanez, H. B. Kichou, J. L. Prego-Borges, J. Salazar, A. Turo, and F. Montero de Espinosa, "Ultrasonic lamb wave NDE system using an air coupled concave array transducer," IEEE Int. Ultrason. Symp. **2**, 1282–1285 (2004).
[30]X. L. Deán-Ben and D. Razansky, "Functional optoacoustic human angiography with handheld video rate three dimensional scanner," Photoacoustics **1**(3), 68–73 (2013).